J. Fluid Mech. (2007), *vol.* 572, *pp.* 231–254.
doi:10.1017/S0022112006003569 Printed in the United Kingdom

Structure of thermal boundary layers in turbulent Rayleigh–Bénard convection

By R. DU PUITS[1], C. RESAGK[1], A. TILGNER[2], F. H. BUSSE[3] AND A. THESS[1]

[1]Department of Mechanical Engineering, Ilmenau University of Technology, P.O. Box 100565, 98693 Ilmenau, Germany

[2]Institute of Geophysics, University of Goettingen, 37075 Goettingen, Germany

[3]Institute of Physics, University of Bayreuth, 95440 Bayreuth, Germany

(Received 30 June 2005 and in revised form 21 July 2006)

We report high-resolution local-temperature measurements in the upper boundary layer of turbulent Rayleigh–Bénard (RB) convection with variable Rayleigh number Ra and aspect ratio Γ. The primary purpose of the work is to create a comprehensive data set of temperature profiles against which various phenomenological theories and numerical simulations can be tested. We performed two series of measurements for air ($Pr = 0.7$) in a cylindrical container, which cover a range from $Ra \approx 10^9$ to $Ra \approx 10^{12}$ and from $\Gamma \approx 1$ to $\Gamma \approx 10$. In the first series Γ was varied while the temperature difference was kept constant, whereas in the second series the aspect ratio was set to its lowest possible value, $\Gamma = 1.13$, and Ra was varied by changing the temperature difference. We present the profiles of the mean temperature, root-mean-square (r.m.s.) temperature fluctuation, skewness and kurtosis as functions of the vertical distance z from the cooling plate. Outside the (very short) linear part of the thermal boundary layer the non-dimensional mean temperature Θ is found to scale as $\Theta(z) \sim z^{\alpha}$, the exponent $\alpha \approx 0.5$ depending only weakly on Ra and Γ. This result supports neither Prandtl's one-third law nor a logarithmic scaling law for the mean temperature. The r.m.s. temperature fluctuation σ is found to decay with increasing distance from the cooling plate according to $\sigma(z) \sim z^{\beta}$, where the value of β is in the range $-0.30 > \beta > -0.42$ and depends on both Ra and Γ. Priestley's $\beta = -1/3$ law is consistent with this finding but cannot explain the variation in the scaling exponent. In addition to profiles we also present and discuss boundary-layer thicknesses, Nusselt numbers and their scaling with Ra and Γ.

1. Introduction

Turbulent thermal convection is the most frequently occurring type of fluid flow in Nature. In spite of its widespread occurrence, the local properties of the temperature and velocity fields in turbulent thermal convection are still poorly understood. Even for the idealized case of Rayleigh–Bénard (RB) convection – the flow in a horizontal fluid layer heated from below and cooled from above – our knowledge is modest in many respects. Referring to temperature and velocity profiles in RB convection, Townsend (1958) wrote almost fifty years ago 'that' the experimental material is very meagre by comparison with our knowledge of the turbulent motion in shear flow'. It is astonishing that this statement is still true today. The purpose of the present work is to bridge this gap by performing local temperature measurements inside the thermal

boundary layers of turbulent RB convection that have a higher spatial resolution than in previous experimental investigations.

Rayleigh–Bénard convection is characterized by three control parameters, namely the Rayleigh number Ra, the Prandtl number Pr and the aspect ratio Γ. The main parameter is the Rayleigh number,

$$Ra = \frac{\gamma g \Delta\vartheta H^3}{\nu\kappa}, \tag{1.1}$$

which describes the ratio of the buoyancy force driving the flow and the viscous and thermal dissipation damping it. In this equation, γ denotes the thermal expansion coefficient, the acceleration due to gravity is represented by g, the temperature difference between the heated bottom plate and the cooled top plate is written as $\Delta\vartheta$ and the distance between the plates is H. Furthermore ν and κ stand for the kinematic viscosity and the thermal diffusivity, respectively. The material properties of the fluid are characterized by the Prandtl number

$$Pr = \frac{\nu}{\kappa}, \tag{1.2}$$

which represents the ratio of the thermal and the viscous time scales. If the fluid were laterally unbounded, Ra and Pr would be the only control parameters. Most experiments, however, are performed in cylinders whose inner diameter D defines the third parameter, the aspect ratio

$$\Gamma = \frac{D}{H}. \tag{1.3}$$

A requirement of fundamental importance in RB convection (Siggia 1994) is to predict and measure the convective heat flux $\dot{q}_k$ and the mean velocity U, as well as their dependence on the parameter set. Usually this is written in the form $Nu(Ra, Pr, \Gamma)$ and $Re(Ra, Pr, \Gamma)$, where the dimensionless Nusselt number Nu and Reynolds number Re are defined via

$$Nu = \frac{\dot{q}_c}{\dot{q}_d}, \qquad Re = \frac{UH}{\nu}. \tag{1.4}$$

Here $\dot{q}_c$ is the convective heat flux, $\dot{q}_d$ is the diffusive heat flux and U is the mean velocity.

The significant progress in our understanding of these scaling laws at very high Rayleigh numbers (Niemela *et al.* 2000; Chavanne *et al.* 2001; Grossmann & Lohse 2000; Verzicco & Camussi 2003) is in contrast with the conspicuous lack of reliable experimental data on the profiles of temperature and velocity for $Ra > 10^{11}$. Despite a considerable number of temperature-profile measurements in the past, the experimental results scatter very strongly. While in early measurements at low Rayleigh numbers a power-law scaling of the temperature in the boundary layer was observed (Prandtl 1932) found $\vartheta \sim z^{-1/3}$ and Malkus (1954*b*) found $\vartheta \sim z^{-1}$), more recent measurements support a logarithmic dependence (see Landau & Lifschitz (1991), who found $\vartheta \sim \ln(z)$ and Chilla *et al.* (1993), who found $\vartheta \sim \int \exp(-z^3)\,\mathrm{d}z$). All these theories could be evaluated experimentally only in a limited range of Ra and z. A similar situation holds in relation to the r.m.s. temperature fluctuation σ, where e.g. regimes of $\sigma \sim z^{-1/3}$ (Priestley 1954) or $\sigma \sim \ln(z)$ (Fernandes & Adrian 2002) have been observed.

Convective heat transfer was first investigated by Prandtl (1932) and Priestley (1954). They considered free convective heat transfer from a single hot plate to

the fluid above it. Prandtl predicted that it depends only on a thin boundary layer attached to the heated plate and is independent of the thickness of the fluid layer above. Then the wall-normal profile of the (potential) mean temperature Θ_p in this layer can be described by a simple power law,

$$\Theta_p(z) \sim z^{\alpha}, \qquad \alpha = -\tfrac{1}{3}. \tag{1.5}$$

Furthermore Priestley showed that, in a region sufficiently far away from the plate to avoid near-wall effects, the variation in the r.m.s. temperature fluctuation σ scales with the wall-normal distance z from the plate as

$$\sigma \sim z^{\beta}, \qquad \beta = -\tfrac{1}{3}. \tag{1.6}$$

His theoretical considerations based on similarity and dimensional analysis were confirmed by the atmospheric measurements of several authors (Best 1935; Rider & Robinson 1951; Ramdas 1953).

A further theory by Malkus for two parallel plates (Malkus 1954*a*, *b*) was based on a nearly isothermal core in the RB cell and two boundary layers with a steep temperature gradient close to the plates. It leads to a power-law behaviour of the mean temperature gradient $\Theta_p(z)$, (1.5), but the exponent α is determined to be -1. The same exponent was predicted by Kraichnan's analysis (Kraichnan 1962), but he found $\alpha = -1/3$ further into the interior of the cell.

In order to check these hypotheses, a considerable number of high-Rayleigh-number experiments in air (Thomas & Townsend 1957; Townsend 1958; Deardorff & Willis 1967; Fitzjarrald 1977) and water (Chu & Goldstein 1973) were performed. Townsend investigated turbulent convection in an open-topped box with a uniformly heated bottom plate and a sidewall 56 cm in height. According to Prandtl's and Priestley's theory the temperature profiles $\Theta_p(z)$ measured at the heating plate for different Ra are represented by a power law, (1.5), but Townsend's exponent varied in a wide range between $-0.3 > \alpha > -1.5$. The r.m.s. temperature fluctuation could also be described by a power law, cf. (1.6), with a scaling exponent $\beta = -0.6$ which considerably differs from the predicted value. Chu & Goldstein (1973) also observed in a water cell heated from below and cooled from above that the temperature Θ_p scaled with z as in (1.5) but, depending on the Ra number ($2.7 \times 10^5 < Ra < 1.0 \times 10^8$), the exponent was determined as $-1 > \alpha > -3$. Fitzjarrald measured the temperature and the velocity field in a large cavity filled with air at larger Rayleigh numbers up to $Ra = 7 \times 10^9$ but he did not analyse the temperature profile near the bounding walls.

Belmonte, Tilgner & Libchbaer (1993, 1994) and Tilgner, Belmonte & Libchbaer (1993) achieved higher Rayleigh numbers in RB cells filled with water (up to $Ra = 10^9$) or with compressed SF_6 (up to $Ra = 10^{11}$). They measured the temperature profile in the wall-normal direction and represented it in a normalized form as

$$\Theta(z) = \frac{\bar{\vartheta}(z) - \bar{\vartheta}_{CP}}{\bar{\vartheta}_{HP} - \bar{\vartheta}_{CP}}, \tag{1.7}$$

where $\bar{\vartheta}(z)$ is the mean temperature at the position z and $\bar{\vartheta}_{HP}$ and $\bar{\vartheta}_{CP}$ are the temperatures of the heating and the cooling plate, respectively. For $Ra < 10^{11}$ they approximated the temperature profile near the wall by a linear function, (1.5) with $\alpha = 1$, assuming a laminar boundary layer at the heating and at the cooling plate. The r.m.s. temperature-fluctuation profile $\sigma(z)$ rose steeply from the surface of the bounding wall up to a maximum which coincided with the intersection point of the gradient of the temperature profile at $z = 0$ and the temperature in the interior of the cell. They defined this point as the edge of the boundary layer. Furthermore they

analysed the decreasing part of the r.m.s. temperature fluctuation and determined the exponent, (1.6), as $\beta = -0.80$ (water) and $\beta = -0.72$ (SF_6). Because of the large size of the sensor relative to the thickness of the boundary layer the spatial resolution of the measurements at large Rayleigh number was limited.

Chilla *et al.* (1993) analysed the profile of the temperature gradient $\partial\Theta/\partial z$ and the r.m.s. temperature fluctuation σ in a large-aspect-ratio cell filled with water ($Ra < 10^8$). They found a logarithmic relation, given by

$$\frac{\partial\Theta(z)}{\partial z} \sim \exp\left(\frac{z^\alpha}{B}\right), \qquad \alpha = -3. \tag{1.8}$$

The profile of the r.m.s. temperature fluctuation $\sigma(z)$ scaled in a logarithmic manner outside the boundary layer, but the coefficients were not given in the paper.

Lui & Xia (1998) reported measurements of the mean-temperature profile in RB convection in a cylindrical water cell. They investigated the scaling properties of the mean-temperature profile and its dependence on Ra in the range $3.4 \times 10^7 < Ra < 4.7 \times 10^{10}$. In their experiment the temperature profiles at different horizontal positions along the large-scale circulation were found to be self-similar when Ra was maintained constant, whereas those measured at different Ra values did not have a universal form. Furthermore they found that the scaling exponent of the boundary-layer thickness δ_Θ varied with Ra depending on the horizontal position.

Fernandes & Adrian (2002) examined the properties of the r.m.s. temperature fluctuation σ and the r.m.s. velocity fluctuation σ_v in a cubic water cell ($\Gamma \approx 10$, $Ra = 10^7$–10^9). The aim of this work was to investigate two versions of the mixing-layer theory of Castaing *et al.* (1989), the so-called λ-I and λ-II theories. In the λ-I theory, the plumes from the plates move through the core without being influenced. Then σ should scale according to (1.6) with $\beta = -1/2$. Otherwise, in the λ-II theory, the plumes are broken down and mixed thoroughly by the turbulent motion in the core and yield a logarithmic scaling of the r.m.s. temperature fluctuation:

$$\sigma \sim \ln(z). \tag{1.9}$$

The experimental results tended to support the second theory, but there were some uncertainties which prevented a final statement.

Another issue to which we intended our experiments to contribute is the unresolved question about the transition of the heat transfer in RB convection to an 'ultimate regime'. This state of the turbulent motion of a fluid was first predicted by Kraichnan (1962) as a regime where the heat transport in the RB cell no longer depends on the fluid properties because of the onset of turbulent mixing in the boundary layer. Regarding the point at which this transition takes place, there are a number of differing theoretical predictions (Kraichnan 1962; Landau & Lifschitz 1991; Grossmann & Lohse 2000) and experimental observations (Castaing *et al.* 1989; Chavanne *et al.* 1997; Niemela *et al.* 2000; Chavanne *et al.* 2001; Niemela & Sreenivasan 2003). Evidence of the so-called ultimate regime in RB convection is still missing. While Niemela found a constant exponent $\eta = 0.309$ over the range of investigated Ra between $10^6 < Ra < 10^{17}$, Chavanne's group observed a transition of the exponent from $\eta = 2/7$ to a higher value at $Ra \approx 10^{11}$. Owing to the complicated experimental conditions in low-temperature helium and the small thickness of the boundary-layer, measurements of temperature and velocity profiles are not possible. Therefore the transition of the boundary layer from laminar to turbulent could not be demonstrated.

The work presented here was motivated by this lack of knowledge about the temperature field in highly turbulent RB convection. In the experimental facility

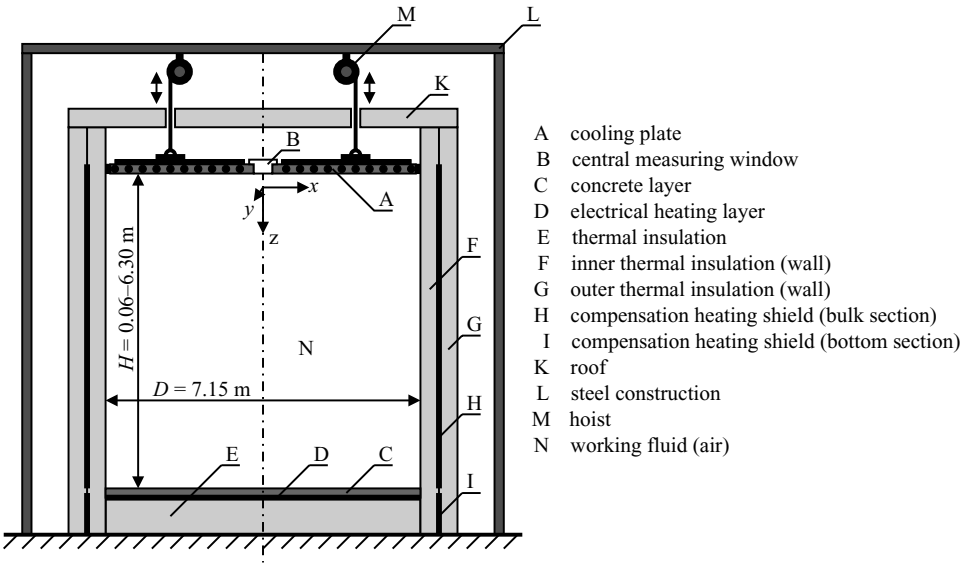

FIGURE 1. The large-scale RB facility (the 'Barrel of Ilmenau').

which we describe in § 2.1, Rayleigh numbers up to $Ra = 10^{12}$ can be achieved. Its large size compared with the small size of our sensors permits temperature and velocity measurements with unprecedented spatial resolution. These data can help us to understand the mechanism of heat transport in highly turbulent convection in more detail. In particular, we address the following two questions.

(i) How do the temperature profile and the heat transport depend on the aspect ratio and the temperature difference of the RB cell?

(ii) Does a variation in the structure of the boundary layer exist at very high Rayleigh numbers indicating a transition towards the so-called ultimate regime?

The paper is divided as follows. In § 2 we describe the experimental facility and the method used for temperature measurements. Section 3 contains results for variable aspect ratio, mainly relating to the first question. In § 4 we investigate the temperature field at $\Gamma = 1.1$ in the range $10^{11} < Ra < 10^{12}$; in this section we focus our special attention onto the second question. In the appendix we discuss heat-flow measurements for both series of experiments.

2. Experimental method and procedures

2.1. *Experimental setup*

We used air as the working fluid and performed our experiments in a large-scale facility, which is shown in figure 1. It consists of a closed cylindrical box (F, K) with an inner diameter $D = 7.15$ m, a heating plate (C, D) at the bottom and a free-hanging cooling plate (A) above. The distance between the heating and cooling plates is continuously adjustable between $H = 0.063$ m and $H = 6.30$ m. The plates are aligned perpendicularly to the vector of the gravitational acceleration, with a deviation smaller than 0.1°. In order to force the convective flow into a certain direction the cooling plate can be inclined to an angle of upto approximately 5°, but we did not make use of this possibility in the experiments reported here. The sidewall is covered with an active compensation heating system (H, I), which is necessary to

suppress lateral heat losses to the environment. The box is filled with ambient air (about 250 m^3 for $\Gamma = 1.13$). Two windows each with diameter 1.00 m and shielded with a separate compensation heating segment can be used for global observation and access for maintenance.

Because our interest was focused on the investigation of the temperature and the velocity field in the vicinity of the cooling plate, we had to guarantee very precise boundary conditions there. For reasons of low weight and good homogeneity of temperature we chose a water-cooled aluminium plate, made of 16 separate segments each covering a sector of angle 22.5°. All segments consist of a lower blank smooth aluminium plate with thickness 6 mm, followed by a cooling-coil system with 25 mm tubes and a second aluminium plate on top. The segments are mounted on a steel rack with total weight approximately 5 tons, which hangs at three hoists M in a steel construction L.

Each segment of the cooling plate is supplied with cooled water by a central cooling system with maximum power 13 kW. A PID controller in combination with a 1 m^3 buffer tank in the cooling circuit guarantees a very stable temperature, which can be adjusted between 15°C and 25°C. The accuracy is better than $\pm 0.1\,^{\circ}C$. In order to achieve intense lateral heat transport and a homogeneous temperature distribution at the plate surface, the highest possible flow rate, approximately 10 $m^3\,h^{-1}$ was chosen and each segment was supplied separately.

The surface temperature of the cooling plate is continuously measured and stored by 19 high-accuracy PT-100 sensors, mounted in holes drilled from the upper site of the plate to about 0.5 mm from its lower surface. Nine sensors are arranged at the ninth segment opposite to the lower maintenance window in a line from the centre of the plate to its outer edge. They give information about the radial distribution of temperature. The other sensors are distributed regularly over the remaining segments. The mean temperature of the cooling plate, $\bar{\vartheta}_{CP}$, which we use for the determination of Ra and for the presentation of non-dimensional temperature profiles is obtained as an average over every second segment.

The construction of the heating system is similar to that of conventional residential underfloor heating. A thermal insulation of polyurethane (E) with thickness 0.3 m and thermal conductivity 0.027 $W\,m^{-1}\,K^{-1}$ reduces the fraction of the heating power flowing from the box into the ground. Written as the ratio of the heat flow through the bottom insulation, $\dot{Q}_G$, and the convective heat flow into the fluid $\dot{Q}_K$, we have $\dot{Q}_G/\dot{Q}_K = 0.04$ for the maximum adjustable temperature difference $\Delta\vartheta_{max} = 60\,K$ between the plates.

Electrical heating wires (D) are mounted in a spiral form at a metal gauze and fixed at the surface of the insulation layer. Both metal gauze and heating wires are poured into a floating floor screed (C) of thickness 5 cm. Its viscosity during manufacture is very small, so a truly plane and horizontally aligned surface is guaranteed. Temperature sensors in the same arrangement as in the cooling plate were embedded 3 mm deep and finally the surface was coated with tinfoil to reduce radiative heat transfer.

The heating system is divided into three concentric sectors with equal areas. The surface temperature of every sector is separately controlled by a PID controller. A mean surface temperature $\bar{\vartheta}_{HP}$ between 80 °C and 20 °C with an accuracy better than $\pm 0.05\,K$ can be adjusted. Because of the nearly constant heat flux from the heating wires and the poor lateral heat transport in the floor screed, the temperature homogeneity of the heating plate is not as good as that of the cooling plate. Areas with higher convective heat flux, e.g. in the centre, or at the edge of the plate, where

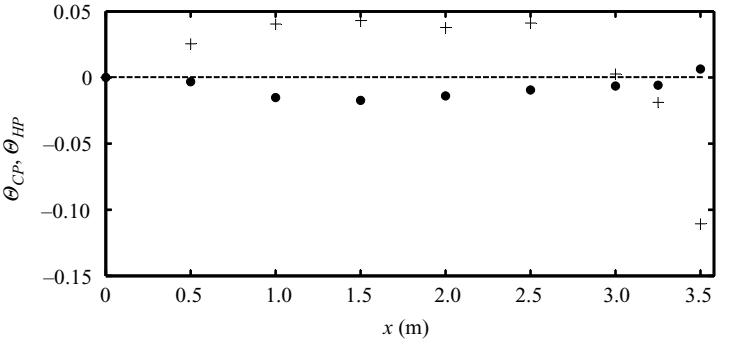

FIGURE 2. Radial uniformity of the thermal boundary conditions: the deviation of the non-dimensional surface temperature of the cooling plate (circles) and the heating plate (crosses) from their mean values. The data given here represent the worst case, where the heating plate is at its maximum temperature, $\bar{\vartheta}_{HP} = 82.5\,^{\circ}\mathrm{C}$ and the cooling plate is at its minimum temperature, $\bar{\vartheta}_{CP} = 18.6\,^{\circ}\mathrm{C}$. The actual experiments were performed at lower temperature differences.

an enhanced heat loss into the ground exist, are colder. Areas with reduced heat flux assume a higher temperature. The different levels of temperature homogeneity of the heating and cooling plate are illustrated in figure 2.

In this figure we plot the radial temperature distribution for the ninth segment of the cooling plate, as well as for the facing side of the heating plate, at the maximum Rayleigh number, $Ra = 10^{12}$. The temperatures in figure 2 are normalized to the temperature difference between the plates according to

$$\Theta_{CP} = \frac{\vartheta_{CP}(x) - \vartheta_{CP}(0)}{\bar{\vartheta}_{HP} - \bar{\vartheta}_{CP}}, \tag{2.1}$$

$$\Theta_{HP} = \frac{\vartheta_{HP}(x) - \vartheta_{HP}(0)}{\bar{\vartheta}_{HP} - \bar{\vartheta}_{CP}}, \tag{2.2}$$

where $\vartheta_{CP}(0)$ and $\vartheta_{HP}(0)$ are the temperatures at the plate centre, $x = 0$. As can be seen the temperature is distributed very homogeneously over the cooling plate and does not deviate by more than 2 % (1.2 K). In comparison, the radial deviation of the heating-plate temperature, particularly at its edge, exceeds this value by a factor 6. In order to reduce the influence of the non-uniform bottom temperature on our local measurements, the latter were conducted exclusively in the upper (cold) boundary layer, where the thermal boundary conditions are well defined.

The sidewall of the experimental facility consists of an inner insulation layer 16 cm thick followed by compensating heating elements and an outer insulation layer with thickness 12 cm. The inner insulating wall is made of five rings of height 1.60 m, each mounted on three 120 ° sections. They consist of an inner and an outer layer of a very stable fibre-reinforced plastic (of thickness 1 cm) as well as an intermediate insulation layer of polyurethane. The heat resistance R_{th} of this simple wall is of the order of $0.04\,\mathrm{K\,W^{-1}}$ and leads to a maximum heat loss $\dot{Q}_W = 1.5\,\mathrm{kW}$ through the sidewall. A compensation heating system (H, I) at the outer surface, covered with additional thermal insulation and finished with an outer weather-resistant plastic board, reduces this heat loss by a factor of about 20. In relation to the convective heat flux at the maximum Rayleigh number ($Ra = 10^{12}$) the lateral heat loss amounts to less than 1 %.

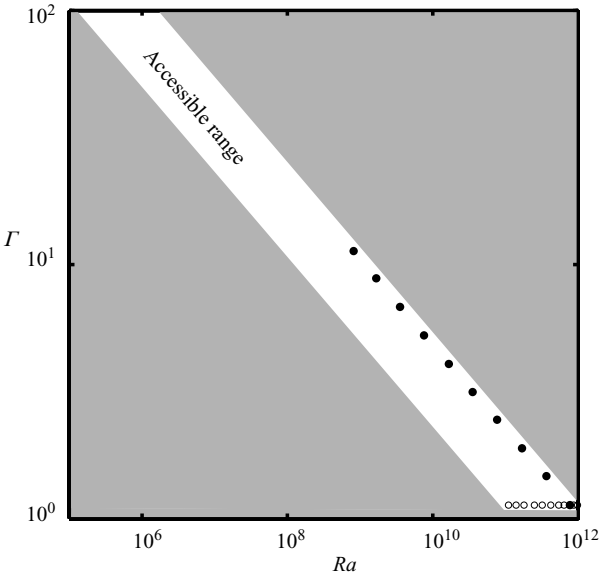

FIGURE 3. Experimental parameters: schematic of the two-dimensional parameter space (Ra, Γ) of our experiment together with the parameters at which measurements were taken. The full circles represent experiments at constant temperature difference and variable aspect ratio (§ 3) whereas the empty circles represent experiments at constant aspect ratio and variable temperature difference (§ 4). The horizontal extent of the parameter space accessible in the experiment is given by the temperature difference $\Delta T = 60\,\mathrm{K}$ at maximum heating power and the minimum temperature difference $\Delta T = 5\,\mathrm{K}$. The upper limit of the aspect ratio is set by the minimum height $H = 0.07\,\mathrm{m}$ below which the deviation of the cooling plate from horizontality, $\Delta H = 5\,\mathrm{mm}$, renders the local Rayleigh number non-uniform.

To avoid computation of a Rayleigh number based on the non-uniform bottom temperature, we define our experimental Ra as

$$Ra = \frac{2\alpha g(\bar{\vartheta}_B - \bar{\vartheta}_{CP})H^3}{\nu\kappa}, \tag{2.3}$$

where $\bar{\vartheta}_B$ is the measured bulk temperature averaged over the time of the profile measurement. All fluid properties are evaluated for this temperature.

In this configuration we were able to investigate thermal convection in a very wide range of parameters, as shown in figure 3. By varying the aspect ratio and the temperature difference between the heating and the cooling plate, the range $5 \times 10^4 < Ra < 10^{12}$ is accessible. Keeping the aspect ratio constant and varying the temperature difference only, the convective flow over approximately one decade in Ra can be examined.

2.2. *Temperature measurements*

The temperature profiles presented here were measured along the central axis of the experiment and our coordinate system is defined as shown in figure 1.

We used a glass-encapsulated microthermistor with a diameter of approximately 140 μm and 18 μm connecting wires. It was supported between the pins of a small transistor case and mounted at the end of a brass tube of diameter 5 mm, as shown in figure 4. Connected to a one-dimensional traverse system, it can be moved in steps of 10 μm along the z-axis. The smallest distance is defined by $z_{min} = 70\,\mu\mathrm{m}$, corresponding

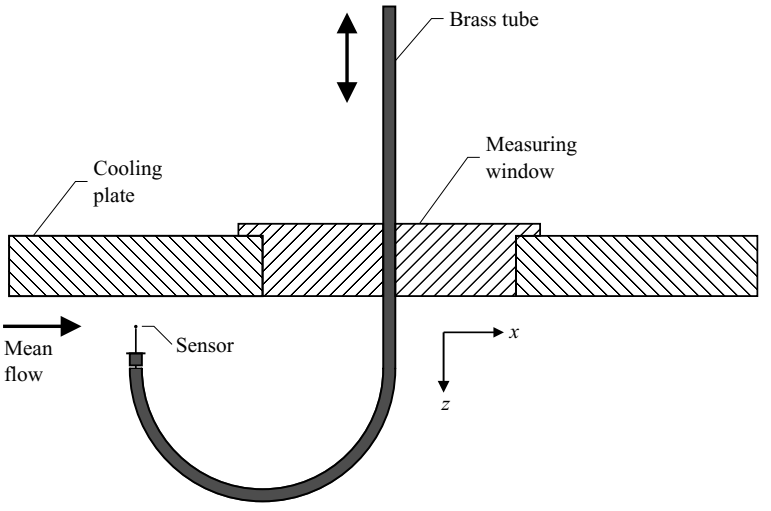

FIGURE 4. Measurement setup: Schematic of the temperature measurement performed through window B (figure 1)

to one-half the sensor diameter. Its basic accuracy was improved by an additional calibration and was better than ± 0.1 K.

In order to prevent measurement errors by self-heating, a measurement current lower than that normally used in commercial instruments is required. The thermal dissipation rate of the thermistor is specified as $\varepsilon_D = 0.045\,\mathrm{mW\,K^{-1}}$ in still air. At a typical resistance of approximately $R_{Th} = 10\,\mathrm{k\Omega}$ at 25 °C and a maximum temperature error $\Delta T = 0.05$ K the current through the sensor must not exceed $I_{Th} = \sqrt{(\varepsilon_D \Delta \vartheta)/R_{Th}} = 10.6\,\mu A$.

Owing to the variation in the current caused by the temperature dependence of the resistance, a lower current, $I_{Th} = 5\,\mu$A, was used in our experiments. The current was supplied by a special resistance bridge with an internal DC-voltage source. The bridge transforms the resistance of the thermistor into a voltage and amplifies it by a factor 100. The output voltage of the bridge is in the range between -10 V and $+10$ V and is measured using a computer-controlled system based on an HP3458. It permits a maximum sampling rate of $333\,\mathrm{s^{-1}}$ with six-digit resolution. The measuring instrument and the traverse system are controlled by the PC, where a LabVIEW program is running. This arrangement permits temperature measurements in air with negligible heating of the sensor, high accuracy and noise immunity as well as excellent long-term stability.

We studied the temperature field at the cooling plate between $z = 0.07$ mm and $z = 150.07$ mm. Measuring the temperature at 39 positions over a time span of one hour for each position and with a sampling rate of $200\,\mathrm{s^{-1}}$, 39 time series of 720 000 temperature values were obtained. Systematic errors created for example by environmental influences were excluded by a random selection of measurement positions. Double measurements at eight points allowed us to estimate the statistical relevance of the recorded data. Before a measurement with new parameters was started, we waited at least 48 hours to achieve a steady state in the RB cell.

In addition to the regular profile measurements described above, one high-resolution temperature profile at $Ra = 7.7 \times 10^{11}$ and $\Gamma = 1.13$ was obtained. We expanded the number of data points from 39 to 77 positions and the measurement time at each

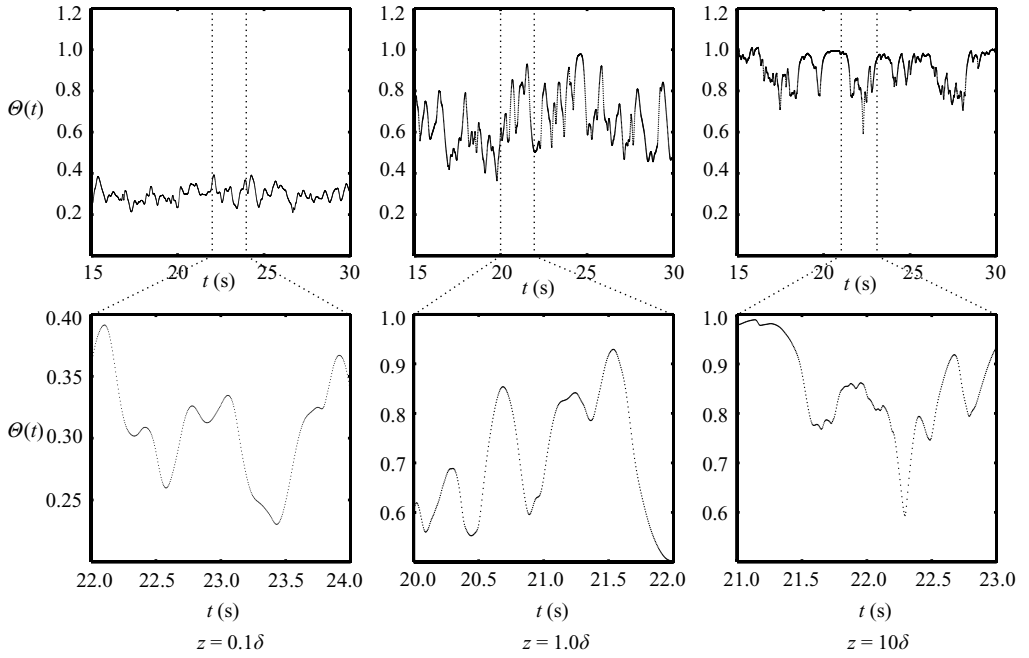

FIGURE 5. Raw data: three examples of temperature time series taken at different distances from the cooling plate for an experiment at $Ra = 7.7 \times 10^{11}$ and $\Gamma = 1.13$.

position from one to two hours. Particularly for the higher statistical moments, the scatter of the calculated profiles could thereby be reduced in comparison with the shorter measurements.

In total, we performed 20 regular series and one extended series of temperature-profile measurements. With a duration of 48 hours per measurements for the regular profiles and 192 hours per measurement for the extended profiles, not forgetting the waiting times needed for the adjustment of thermal conditions, it took approximately 21 weeks for the reported measurements to be completed.

In order to demonstrate the high temporal resolution of the temperature measurements, three examples of temperature time series at different z-positions are shown in figure 5. The experimental parameters are adjusted to $\Gamma = 1.13$ and $Ra = 7.7 \times 10^{11}$. In the diagrams the normalized temperature

$$\Theta_i(z) = \frac{\vartheta_i(z) - \bar{\vartheta}_{CP}}{\bar{\vartheta}_B - \bar{\vartheta}_{CP}} \tag{2.4}$$

is plotted over a time interval of 15 s. The value $\Theta = 0$ corresponds to the temperature of the cooling plate $\bar{\vartheta}_{CP}$ and the value $\Theta = 1$ is the mean temperature halfway between the heating and the cooling plate which is often referred to as the bulk temperature $\bar{\vartheta}_B$. The time series were sampled at a standard rate of $200\,\mathrm{s}^{-1}$ at three distances, $z = 0.1\delta_\Theta$ (0.3 mm); $z = 1.0\delta_\Theta$ (3 mm) and $z = 10\delta_\Theta$ (30 mm); the thickness of the thermal boundary layer δ_Θ is defined below. Good temporal resolution is visible particularly in the lower windows, where the time scale is stretched.

At the smallest distance from the cooling plate, corresponding to the left-hand plots in figure 5, the mean temperature $\Theta(z)$ is about 0.3. The fluctuations are very small and uniformly distributed around the mean value. All data are presented and analysed without any kind of filtering. The mean temperature at $z = 1.0\delta_\Theta$ amounts

to $\Theta(z) = 0.7$. The fluctuations at this point are considerably larger but they are still distributed uniformly around the mean. At a distance of $z = 10\delta_\Theta$, the normalized mean temperature is close to the bulk temperature $\Theta(z) = 1.0$ but with strong negative spikes. In contrast with the position at the boundary layer, a number of positive spikes with $\Theta(z) > 1.0$ caused by hot plumes can be registered. However, the temperature of the positive spikes in the complete time series of two hours did not exceed $\Theta_{max} = 1.08$, indicating that thermals or plumes from the heating plate are mixed and cool down very strongly during their upward travel.

From these time series the profiles of the normalized mean temperature $\Theta(z)$, the standard deviation std(z) and the dimensionless r.m.s. temperature fluctuation $\sigma(z)$ normalized by the temperature difference between the bulk temperature $\bar{\vartheta}_B$ and the temperature of the cooling plate $\bar{\vartheta}_{CP}$ were computed. Furthermore we analysed the skewness $s(z)$ and the kurtosis $k(z)$.

We characterize the near-wall behaviour of our temperature profiles by defining four length scales, namely $\delta_\Theta = (d\Theta/dz|_{z=0})^{-1}$, $\delta_\sigma = \{z : d\sigma/dz = 0\}$, $\delta_s = \{z : s(z) = 0\}$ and $\delta_k = \{z : k(z) = 3\}$. The first quantity is the usually defined thickness of the thermal boundary layer, based on the slope of the temperature profile at the wall. Since our mean-temperature profiles show only a short linear part, we first fitted the temperature in the range $0 < z < 2.07$ mm by the function $\Theta(z) = az^2 + bz + c$ and then computed $\delta_\Theta = 1/b$. The second boundary-layer thickness δ_σ is defined by the point at which the temperature fluctuations reach their maximum. The quantities δ_s and δ_k define the positions where the probability distribution of the temperature has zero skewness and has the same kurtosis as a normal distribution, respectively.

Before proceeding to a discussion of the results we would like to emphasize that we have not plotted our temperature data in terms of non-dimensional 'wall variables' (cf. Townsend 1958). The introduction of such quantities requires an accurate knowledge of the heat flux. Since our facility was not designed for high-accuracy Nusselt-number measurements, the utilization of experimental heat-flux data would introduce an additional source of uncertainty and reduce the reliability of our profiles. Moreover, the heat flux is spatially nonuniform for most high-Rayleigh-number experiments, including ours. Under such circumstances the global heat flux may not be a reliable quantity for non-dimensionalization.

3. Results for variable aspect ratio

In the first series of measurements we fixed the temperature difference and studied the temperature field for 10 different heights of the cooling plate. Small deviations of the temperature of the heating plate and of the bulk temperature (table 1) are caused by the averaging of the inhomogeneous temperature distribution at the surface of the heating plate. As shown in figure 3, this parameter set corresponds to a movement along the downward sloping curve $\Gamma = \text{const} \times Ra^{-1/3}$ in our two-dimensional parameter space (Ra, Γ). The exact values of the parameters are listed in table 1.

We start our discussion with an analysis of the profiles of the mean temperature $\Theta(z)$, the r.m.s. temperature fluctuation $\sigma(z)$, the skewness $s(z)$ and the kurtosis $k(z)$. Before we turn to a comparison of the temperature fields for different values of Γ, we will analyse the most interesting case, that of minimum aspect ratio $\Gamma = 1.13$ and maximum Rayleigh number $Ra = 7.69 \times 10^{11}$. From previous measurements and from theoretical predictions a laminar boundary layer with a linear temperature profile was expected, but the measurements gave quite different results.

Ra	Γ	$\bar{\vartheta}_{HP}$(°C)	$\bar{\vartheta}_{B}$(°C)	$\bar{\vartheta}_{CP}$(°C)
8.14×10^8	11.3	62.95	42.71	20.06
1.67×10^9	8.83	62.64	41.68	20.08
3.54×10^9	6.81	62.64	40.80	20.08
7.56×10^9	5.26	62.78	40.28	20.08
1.66×10^{10}	4.06	63.18	40.62	20.07
3.53×10^{10}	3.15	62.78	40.36	20.08
7.66×10^{10}	2.45	63.08	40.95	20.08
1.69×10^{11}	1.89	62.86	41.23	20.06
3.66×10^{11}	1.47	63.61	41.68	20.07
7.69×10^{11}	1.13	65.00	40.82	20.07

TABLE 1. Set of parameters for the variable-aspect-ratio measurement series.

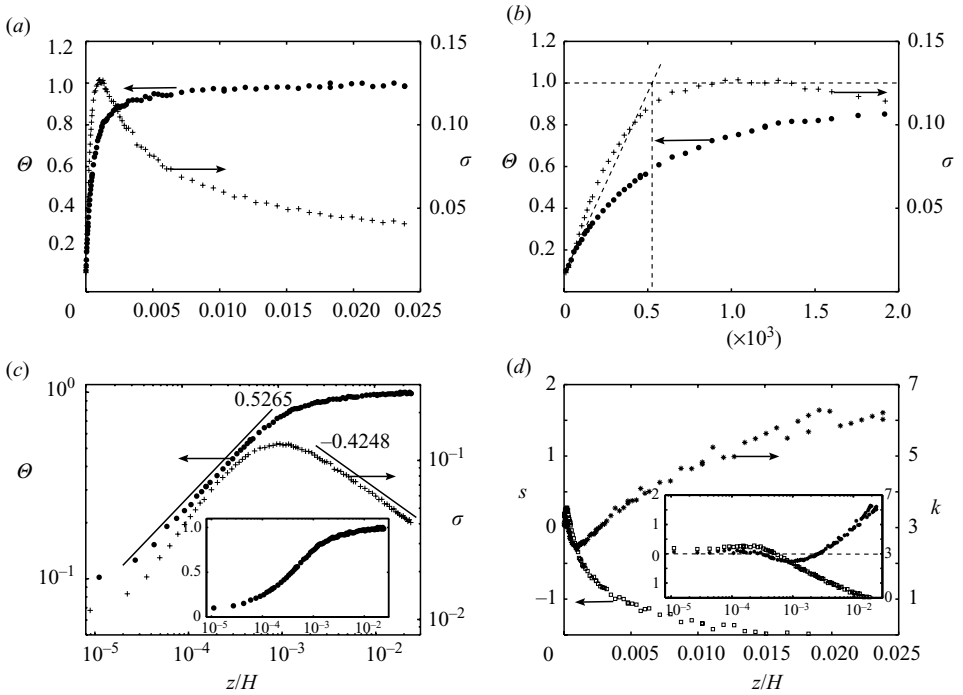

FIGURE 6. Profiles for the parameter set $Ra = 7.7 \times 10^{11}$ and $\Gamma = 1.13$: (*a*)–(*c*) the mean temperature Θ (circles) and the r.m.s. temperature fluctuation σ (crosses); (*d*) profiles of skewness s (squares) and kurtosis k (stars). The insets in (*c*) and (*d*) are semilogarithmic plots of Θ and the profiles of s and k, respectively.

Both the mean-temperature profile and the profile of the r.m.s. temperature fluctuation are plotted in figure 6(*a*) versus the normalized distance z/H. At first glance they do not differ from previous measurements. The temperature $\Theta(z)$ and the fluctuations $\sigma(z)$ rise very quickly in a thin layer below the plate. While the temperature tends to the bulk temperature, the fluctuation first attains a maximum and then decreases with increasing distance from the cooling plate. However, looking more carefully at the immediate vicinity of the plate (figure 6*b*), two remarkable differences from previous temperature measurements become visible.

Although our measurements probe the thermal boundary layer with much higher spatial resolution than that in previous RB experiments, our mean temperature does not converge exactly toward the temperature of the cooling plate as $z \to 0$. This can be inferred from the fact that the extrapolation of the curve $\Theta(z)$ in figure 6(*b*) to $z = 0$ crosses the vertical axis at $\Theta > 0$ rather than $\Theta = 0$. This effect, which does not occur for lower Rayleigh numbers (cf. § 4 below) and which was not noticed in previous investigations owing to limited spatial resolution, is a consequence of the finite size of our sensor and its interaction with the mean flow and the cooling plate. Indeed, when the distance between the sensor and the cooling plate becomes comparable with the size of the sensor (which certainly is the case for $z < 0.6\,\mathrm{mm}$ ($z/H < 10^{-4}$)), its presence distorts the flow. This leads to a stagnant zone between the sensor and the plate, associated with a low heat-transfer coefficient, and to an accelerated flow on the opposite side of the sensor, associated with a high heat-transfer coefficient. Such asymmetry in the thermal boundary conditions at the sensor results in a vertical heat flux through the sensor, whose thermal conductivity is much higher than that of air, and gives rise to a higher apparent temperature. Notice that even in its closest position to the cooling plate the sensor is surrounded by a strong velocity gradient, whose value was estimated from preliminary laser-Doppler velocimetry measurements as $\mathrm{d}U/\mathrm{d}z \approx 240\,\mathrm{s}^{-1}$. Additional errors due to radiative heat transfer from the sensor to the cooling plate are possible. However, this effect should have the opposite sign.

The second remarkable observation is the virtual absence of a linear part in the mean temperature profile. This observation is in contrast with previous temperature measurements at lower Rayleigh number, such as those of Deardorff & Willis (1967) and Townsend (1958) in air for $Ra < 10^7$ and those of Belmonte *et al.* (1994) in high-pressure gases for $Ra = 3.5 \times 10^9$. In the latter experiment the linear part of the profile extended down to $z/H = 0.003$, but this part was covered by only five measurement points. Up to now, direct numerical simulations have not been capable of reliably predicting the details of the temperature profiles near the plates for the Rayleigh numbers of our experiment. In our mean-temperature profile (figure 6*a*) only a small layer up to $z/h \approx 6 \times 10^{-5}$ ($z = 0.37\,\mathrm{mm}$) shows a linear dependence. A curvature is already noticeable when $\Theta(z)$ reaches 30 % of its bulk value. Invoking the results of preliminary mean-velocity measurements, we can identify the linear part as the small viscous (laminar) sublayer. The tangent to this part of the mean-temperature profile defines the thickness of the thermal boundary layer δ_Θ, as shown in figure 6(*b*). Belmonte *et al.*'s hypothesis that $\delta_\Theta = \delta_\sigma$, where δ_σ is the point of maximum r.m.s. temperature fluctuation, is not confirmed by our measurements, as seen in figure 6(*b*). Over the large range between $z/H = 5 \times 10^{-5}$ ($z = 0.32\,\mathrm{mm}$) and $z/H = 8 \times 10^{-4}$ ($z = 5.04\,\mathrm{mm}$) we found that the scaling of the mean temperature with distance can be fitted very well by the power law

$$\Theta(z) = C(z/H)^\alpha, \qquad C = 31.56,\ \alpha = 0.5265. \tag{3.1}$$

This region is limited from below by the viscous sublayer and from above by the edge of the thermal boundary layer. The behaviour of the mean-temperature profile corresponds to the theories of Prandtl, Priestley and Malkus but the exponent differs from the predicted values. The plot of the mean-temperature profile in a semilogarithmic scaling, shown as an inset in figure 6(*c*), demonstrates that there is no pronounced logarithmic behaviour. The exponents involving the other parameters are listed in table 2.

Another often-examined aspect is the decay of the r.m.s. temperature fluctuation σ after it has reached its maximum. A number of predictions ranging from a power-law behaviour with exponents between $\beta = -1/3$ and $\beta = -1/2$ (see (1.6) (Priestley 1954;

Γ	α	β	σ_{max}	δ_Θ (mm)	δ_σ (mm)	δ_s (mm)	Nu
1.13	0.527	−0.425	0.127	3.29	6.67	3.32	587
1.47	0.473	−0.387	0.122	2.85	6.87	2.93	436
1.89	0.484	−0.323	0.131	3.08	6.28	3.60	339
2.45	0.469	−0.324	0.132	3.17	6.22	3.58	269
3.15	0.530	−0.305	0.135	3.13	6.22	3.42	221
4.06	0.497	−0.320	0.135	3.00	5.70	3.31	172
5.26	0.512	−0.302	0.138	3.09	5.71	3.57	137
6.61	0.538	−0.324	0.147	3.12	5.69	3.35	103
8.83	0.550	−0.367	0.148	2.92	4.85	3.19	77
11.3	0.551	−0.370	0.153	2.85	4.67	2.97	58

TABLE 2. Measurement data for the variable-aspect-ratio series.

Castaing *et al.* 1989) to a logarithmic scaling (Fernandes & Adrian 2002) exist and our measurements add an additional piece to this puzzle. Our data can be described by a power law too but the exponent varies in the range $-0.302 > \beta > -0.425$ depending on the aspect ratio Γ, the lowest value being measured at the lowest Γ.

Having discussed the profiles of mean temperature and temperature fluctuation we now turn to the profiles of the higher-order moments, namely the skewness $s(z)$ and the kurtosis $k(z)$, plotted in figure 6(*d*).

The measured skewness profile is characterized by two regions. In the first, ranging from $z/H = 0$ ($z = 0$ mm) to $z/H = 5 \times 10^{-4}$ ($z = 3.2$ mm), the skewness is small but weakly positive. This is a consequence of the fact that the temperature is bounded from below by $\Theta_{min} = 0$. The symmetrical distribution of the temperature fluctuations inside this region indicates that cold fluctuations from the cooling plate and hot fluctuations from the bulk are balanced. In the second region, from $z/H = 5.0 \times 10^{-4}$ ($z = 3.2$ mm) up to the maximum measurement distance $z/H = 2.4 \times 10^{-2}$ ($z = 150$ mm), the skewness drops, intersect the x-axis and seems to move towards an asymptotic value of $s = -2$ far away from the plate. This observation agrees with measurements of Castaing *et al.* (1989), who found that the temperature samples in the bulk are distributed exponentially in the hard turbulent regime ($Ra > 10^8$).

In the kurtosis profile the sharp difference between the boundary layer and the bulk region is reflected as well. In the boundary layer the temperature samples are close to the Gaussian distribution ($k = 3$). After a small drop to values $k < 3$ the kurtosis rises to a value $k > 6$. Because of the limited maximum-measurement distance, $z < 150$ mm, a general statement about the behaviour in the bulk region cannot be made.

In figure 7 the values of δ_Θ and δ_σ may be compared as functions of the aspect ratio; the first quantity is defined by the slope of the mean temperature at $z = 0$ and the second quantity is based on the z-position of the maximum r.m.s. temperature fluctuation. Between its lowest and highest values the thickness δ_Θ varies only by about 0.4 mm, which is about 10 % and inside the measurement and calculation error. In contrast with this observation, δ_σ depends on the aspect ratio. Surprisingly, the z-position does not change continuously with the aspect ratio; rather we found different bands in which the boundary-layer thickness remains nearly constant. The results are summarized in table 2.

Obviously the boundary-layer thickness δ_σ is more influenced by the global flow structure than by the boundary-layer conditions. As we know, a large single roll exists at $\Gamma = 1.13$ and we assume that a transition to other modes occurs for higher

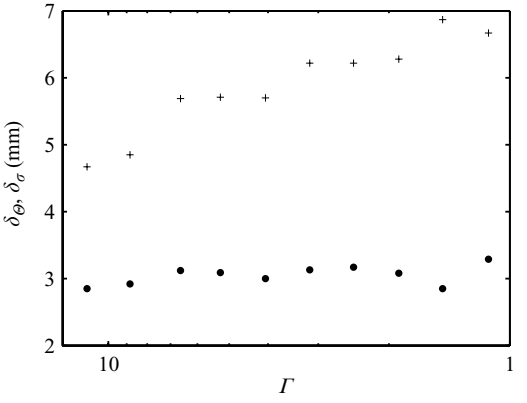

FIGURE 7. Boundary-layer thicknesses for variable aspect ratio as obtained from the slope of the mean temperature Θ near $z=0$ (δ_Θ, solid circles) and from the location of the maximum of the r.m.s. temperature fluctuation (δ_σ, crosses). The exact values of the data are given in table 2.

Γ. For example, during preliminary flow visualization at $\Gamma=2$ we observed a flow change from one large single roll to a double-roll structure and back again. This fact corresponds with the first transition of δ_σ between $\Gamma=1.47$ and $\Gamma=1.89$ (table 2). Increasing Γ again, a second change between $\Gamma=3.15$ and $\Gamma=4.06$ and a third one between $\Gamma=6.61$ and $\Gamma=8.83$ occurred. Niemela & Sreenivasan (2005) reported experiments in an RB cell with $\Gamma=4$ for $Ra=6.5\times10^{11}$: they found that the mean circulation vanishes for aspect ratios larger than unity. Presently we do not know enough about how the geometry influences the global flow structure and how to interpret the effects mentioned above. Some clarification of this issue can be expected from ongoing local and global measurements of the velocity field and from global-flow visualization.

The next interesting issue especially regarding the heat transport is to compare the shapes of the mean-temperature profiles. If the relation $Nu\sim Ra^{1/3}$ is true then both the heat flux $\dot{Q}_K$ and the thickness of the boundary layer δ_Θ should be independent of the distance between the heating and cooling plates. We plot four examples of the mean-temperature profile scaled by δ_Θ in figure 8(a). From the lowest aspect ratio, $\Gamma=1.13$ ($Ra=7.7\times10^{11}$), up to the highest, $\Gamma=11.3$ ($Ra=8.1\times10^{8}$), (cf. figure 7), no significant difference between the profiles can be discerned. Both the slope of the profile and the boundary-layer thickness δ_Θ depend on the aspect ratio only weakly.

A comparison of the corresponding profiles of the temperature fluctuation σ (figure 8b) confirms the weak dependence of the boundary-layer structure. Only the values of the maximum fluctuation σ_{max} differ slightly (table 2). The highest value was measured at $\Gamma=11.3$ ($Ra=8.1\times10^{8}$), which is perhaps an indication of a more unstable and irregular flow at large aspect ratios. In figures 8(c), (d) the skewness and kurtosis profiles, respectively, are shown. Inside the boundary layer the temperature samples are distributed almost normally around the mean and also remain unchanged for the parameter range investigated. All the skewness profiles, and the kurtosis profiles as well, coincide inside the boundary layer. The skewness intersects the x-axis at $z/\delta_\Theta\approx1$, indicating the association of this value with the boundary-layer thickness δ_Θ. With increasing distance from the cooling plate the profiles spread. For the smallest aspect ratio, $\Gamma=1.13$ ($Ra=7.7\times10^{11}$), they decrease logarithmically (see the inset in figure 8c) and approach $s=-2$. This value coincides

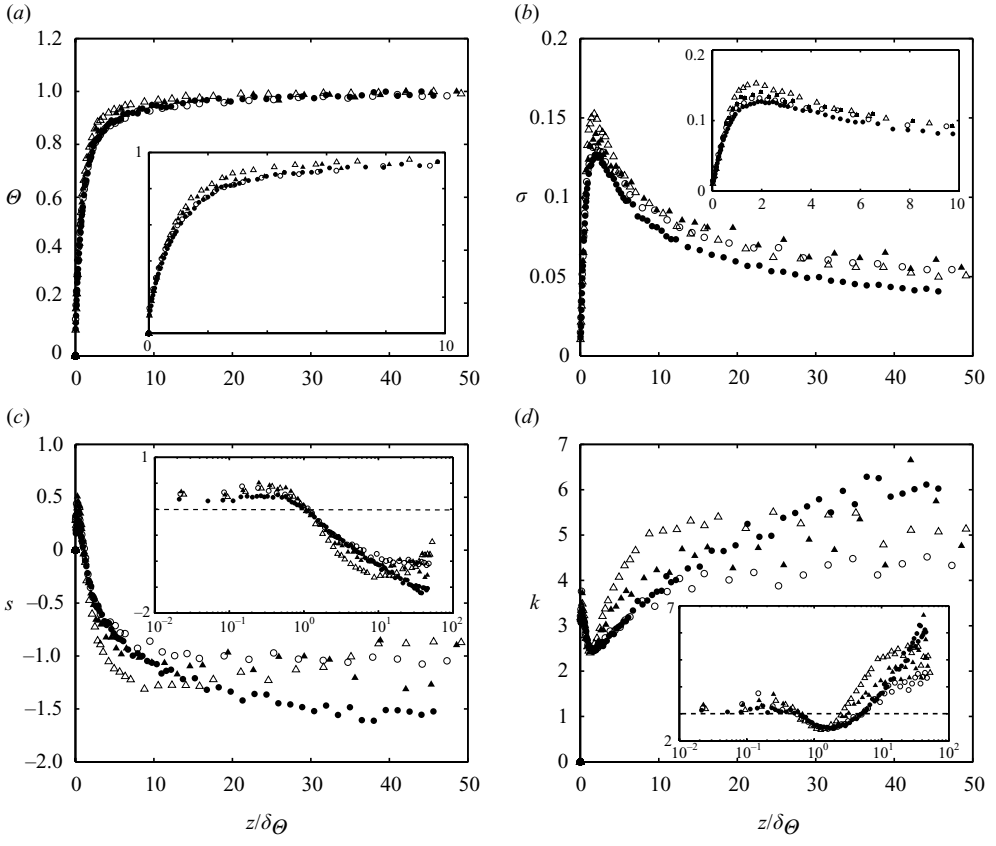

FIGURE 8. The thermal boundary layer for variable aspect ratio. (*a*) Profiles of the mean temperature, (*b*) the r.m.s. temperature fluctuations, (*c*) the skewness and (*d*) the kurtosis for aspect ratios $\Gamma = 1.13$ (solid circles), $\Gamma = 2.45$ (empty circles), $\Gamma = 5.26$ (solid triangles) and $\Gamma = 11.3$ (empty triangles). The insets show the profiles in the immediate vicinity of the cooling plate.

with the measurements of Castaing *et al.* (1989) in the hard turbulent regime. The other profiles at higher aspect ratios do not show a clear trend. As far as we can assess it, the skewness tends to -1 at the maximum measurement distance, corresponding to a distribution of the temperature samples somewhere between the normal and the exponential one. A similar behaviour can be observed in the kurtosis profiles (figure 8*d*). They collapse inside the boundary layer but spread outside it. A clear tendency cannot be detected. The profiles for the higher aspect ratios seem to approximate values lower than $k = 6$ with increasing distance from the cooling plate. Only the profile at $\Gamma = 1.13$ exceeds $k = 6$, with a relatively steep gradient. Possibly it reaches $k = 9$ inside the bulk ($k = 9$ is the characteristic value for exponentially distributed samples), but in fact we were not able to measure it.

4. Results for constant aspect ratio

In this section we set the aspect ratio to its lowest possible value, $\Gamma = 1.13$, and focus our interest on the second question outlined in the introduction: does a variation in the structure of the thermal boundary layer exist in RB convection at high Rayleigh

Ra	$\bar{\vartheta}_{HP}$(°C)	$\bar{\vartheta}_{B}$(°C)	$\bar{\vartheta}_{CP}$(°C)
1.09×10^{11}	24.00	22.23	20.00
1.42×10^{11}	25.70	22.95	20.01
1.86×10^{11}	27.50	23.92	20.01
2.48×10^{11}	31.25	25.33	20.01
3.36×10^{11}	34.40	27.46	20.02
4.19×10^{11}	38.90	29.65	20.04
5.42×10^{11}	45.70	33.15	20.03
6.37×10^{11}	52.20	36.18	20.05
7.69×10^{11}	65.00	40.82	20.07
8.59×10^{11}	70.00	44.62	20.07
9.80×10^{11}	80.40	47.87	18.60

TABLE 3. Set of parameters for the constant-aspect-ratio, $\Gamma = 1.13$, measurement series.

Ra	α	β	σ_{max}	δ_{Θ} (mm)	δ_{σ} (mm)	δ_{s} (mm)	Nu	η_{eff}
1.09×10^{11}	0.758	−0.441	0.145	5.99	16.03	7.91	293	0.6075
1.42×10^{11}	0.626	−0.464	0.146	5.12	13.75	7.29	346	0.3537
1.86×10^{11}	0.583	−0.470	0.145	4.79	12.26	6.31	355	0.1627
2.48×10^{11}	0.542	−0.441	0.139	4.94	10.20	5.60	380	0.2817
3.36×10^{11}	0.544	−0.455	0.138	4.54	9.68	4.71	419	0.3298
4.19×10^{11}	0.535	−0.439	0.135	4.05	8.89	4.32	448	0.2979
5.42×10^{11}	0.523	−0.433	0.131	3.84	8.26	4.00	484	0.3213
6.37×10^{11}	0.517	−0.418	0.128	3.63	7.89	3.86	513	0.5331
7.69×10^{11}	0.526	−0.425	0.124	3.29	6.77	3.31	585	0.5480
8.59×10^{11}	0.496	−0.420	0.124	3.38	6.48	3.36	601	0.5169
9.80×10^{11}	0.481	−0.426	0.117	3.09	6.26	3.24	658	0.6984

TABLE 4. Measurement data for the constant-aspect-ratio, $\Gamma = 1.13$, series.

numbers? Particularly, we relate our measurements to the question whether first signatures for the transition to an 'ultimate regime' can already be observed at a lower Rayleigh number than that predicted by Kraichnan (1962) and Grossmann & Lohse (2000). Inspired by the different results of both the Grenoble experiment (Chavanne *et al.* 1997) and the Oregon experiment (Niemela *et al.* 2000), we conducted a series of heat-flow and temperature-profile measurements at constant aspect ratio, $\Gamma = 1.13$, and varying temperature differences in the range $10^{11} < Ra < 10^{12}$. The complete set of parameters is shown in table 3 and the results are summarized in table 4. It should be noted at this point that the bulk temperature could not be kept constant during all the measurement series and the results at the highest three Rayleigh numbers at least might have been influenced by non-Boussinesq effects.

As shown in figure 11 below, the effective exponent η_{eff} in the relationship between Ra and Nu does indeed increase from $\eta_{eff} \approx 1/3$ for lower Ra (except for the lowest Ra at which the errors are very high) to a significantly higher value for $Ra > 7 \times 10^{11}$. In order to check a possible transition to a turbulent boundary layer we first compared all profiles of the mean temperature Θ and plotted them for three selected Rayleigh numbers, $Ra = 1.1 \times 10^{11}$, $Ra = 3.4 \times 10^{11}$ and $Ra = 9.8 \times 10^{11}$. Because the height (and thereby the aspect ratio) was maintained constant, the distance z is normalized by the height of the RB cell, H, and is plotted as a function of z/H. In the doubly logarithmic representation in figure 9(a) the curve of the mean-temperature profile at the lowest Rayleigh number, $Ra \approx 10^{11}$, starts exactly from the origin of the surface

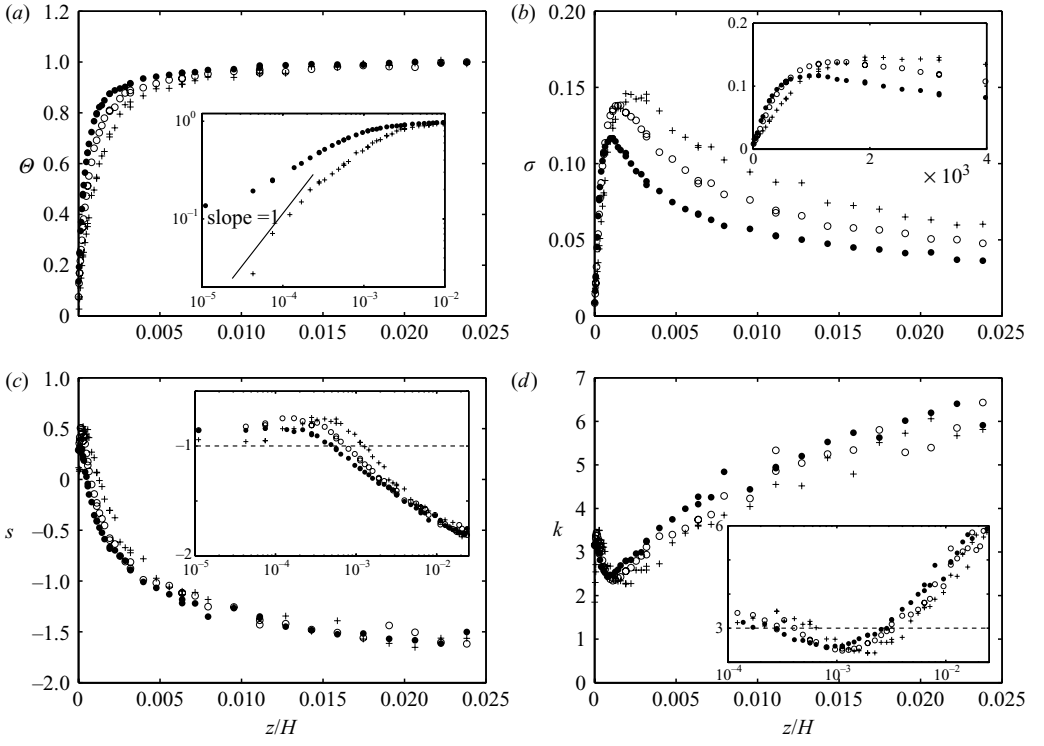

FIGURE 9. Profiles at constant aspect ratio. (*a*) The mean temperature, (*b*) the r.m.s. temperature fluctuation, (*c*) the skewness and (*d*) the kurtosis for $Ra = 1.09 \times 10^{11}$ (crosses), $Ra = 3.36 \times 10^{11}$ (empty circles) and $Ra = 9.8 \times 10^{11}$ (solid circles); $\Gamma = 1.13$. The insets show the behaviour of the profiles in the immediate vicinity of the cooling plate.

temperature (i.e. $\Theta(0) = 0$) and with a linear dependence of Θ on z (corresponding to a slope close to unity in the doubly logarithmic inset of figure 9*a*); the profile at the highest Rayleigh number, $Ra \approx 10^{12}$, starts at a temperature $\Theta(0) \neq 0$ that is noticeably above the surface temperature and with a smaller slope. Further away from the wall, the profiles differ again but approach the asymptotic value $\Theta = 1$ far away from the boundary layer. These effects could be first indications of the transition from a laminar boundary layer, existing only at a very low temperature difference, towards another type. However, the logarithmic mean-temperature profile characterizing a turbulent boundary layer is missing again.

The absence of any transition is also reflected in the profiles of the r.m.s. temperature fluctuation $\sigma(z)$ shown in figure 9(*b*), the skewness $s(z)$ (figure 9*c*) and the kurtosis $k(z)$ (figure 9*d*). With increasing Ra the maximum of σ decreases and its position moves towards the plate. Furthermore, the profile of σ in the vicinity of the cooling plate seems to evolve from a near-linear one at $Ra = 10^{11}$ to an increasingly nonlinear one as Ra rises. This is clearly seen in the inset in figure 9(*b*).

The change in the skewness profile can be observed particularly well in the modification of δ_s. This point, where positive and negative fluctuations are balanced, moves towards the plate. All profiles coincide at the maximum distance from the plate with the value $s = -1.5$. Regarding the profiles of the kurtosis the picture is similar. Both the first and the second intersection point of the profile are shifted toward the cooling plate with increasing Ra. Further into the bulk all profiles seem

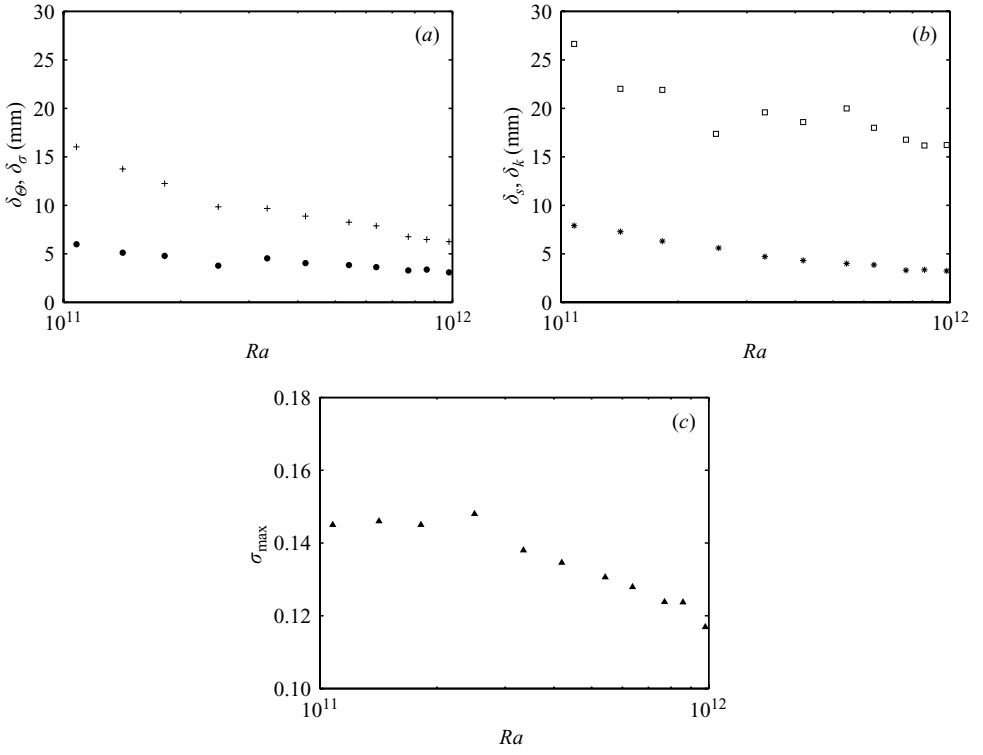

FIGURE 10. Scaling of the boundary-layer thickness at constant aspect ratio $\Gamma = 1.13$. (*a*) The boundary-layer thickness δ_Θ based on the slope of $\Theta(z)$ in the vicinity of the cooling plate and the boundary-layer thickness δ_σ based on the maximum of $\sigma(z)$, (*b*) the boundary-layer thickness δ_s based on the point at which $s(z) = 0$ and the boundary-layer thickness δ_k based on the point at which $k(z) = 3$ and (*c*) σ_{max}.

to approach the same value, $k > 6$, indicating an exponential distribution of the temperature samples and characterizing the hard turbulent regime, as proposed by Castaing *et al.* (1989).

Summarizing the appearance of the profiles in figure 9, it can be stated that all characteristic length scales in the thermal boundary layer continuously decrease with increasing Ra, as expected. In particular, no indications for a sudden transition in the structure of the boundary layer are visible. A more systematic study of the evolution of the profiles, by investigation of the dependence of the characteristic parameters (listed in table 4) on Ra, is possible.

Let us continue by discussing the boundary-layer thickness δ_Θ as a function of Ra, as shown in figure 10(*a*). In contrast with the first series of experiments where δ_Θ does not depend on the aspect ratio or on the Rayleigh number, respectively (§ 3), here it drops weakly with increasing Ra when the temperature difference between the plates is varied while the aspect ratio is kept constant. The dependence can be described by a power law:

$$\delta_\Theta = C_1 Ra^{\mu_1}, \qquad \mu_1 = -0.2540. \tag{4.1}$$

Next we consider the boundary-layer thickness based on the position of the maximum temperature fluctuations, δ_σ (figure 10*a*). It drops even faster, to a value of approximately one-third of its maximum value, and also clearly scales with Ra in

the form of a power law:

$$\delta_\sigma = C_2 Ra^{\mu_2}, \quad C_2 = 4.507 \times 10^5, \quad \mu_2 = -0.4051. \tag{4.2}$$

Obviously the two exponents μ_1 and μ_2 differ strongly. This difference was already observed in our first series of measurements and clearly contradicts the hypothesis of Belmonte *et al.* (1994) according to which $\delta_\Theta = \delta_\sigma$.

The dependence of δ_s on Ra, where δ_s denotes the z-position of vanishing skewness, is similar to that of δ_σ and can be also approximated by a power law:

$$\delta_s = C_3 Ra^{\mu_3}, \quad C_3 = 3.684 \times 10^5, \ \mu_3 = -0.4229. \tag{4.3}$$

Although the second intersection point δ_k of the kurtosis profile also moves towards the plate with increasing Ra its dependence is much weaker than the dependence of the points discussed before (figure 10*b*). Nevertheless, again we express it by a power law:

$$\delta_k = C_4 Ra^{\mu_4}, \quad C_4 = 2.001 \times 10^3, \ \mu_4 = -0.1779. \tag{4.4}$$

Here the coefficient C_4 and the exponent μ_4 are clearly reduced in comparison with the values in the equations above, (4.2), (4.3). Up to this point we can conclude that the thickness and the structure of the boundary layer in the centre of the cooling plate change continuously in the parameter range investigated. Just as stated in the discussion of the temperature profiles, the indication of a clear transition of the boundary layer structure is missing, though we obtained evidence of a transition in the convective heat transfer (see the appendix). Apparently the observed rise in the exponent of the global heat transfer is caused by non-Boussinesq effects or a variation in the properties of the fluid.

In order to check this hypothesis, finally we studied $\sigma_{max} = \sigma(\delta_\sigma)$ as a function of Ra (figure 10*c*). Below $Ra = 3 \times 10^{11}$ it remains nearly constant at $\sigma_{max} = 0.145$ while above this value it starts to drop. The point of the transition roughly coincides with the change in the exponent in the $Nu(Ra)$ power law. But since σ_{max} is related to the global flow structure rather than to the structure of the boundary layer we cannot regard this fact as evidence for a new regime of the turbulent heat transport.

5. Conclusions

In this work, high-resolution local-temperature measurements in a large-scale RB experiment, the 'Barrel of Ilmenau', have been presented. Particular attention has been focused on the thickness and structure of the thermal boundary layer at the cooling plate and their influence on the global heat transfer. For Rayleigh numbers up to 10^{12} we measured highly resolved temperature profiles along the central axis of the RB cell and analysed the statistics.

Two series of experiments were carried out, in each of which only a single parameter was varied. In the first series the aspect ratio was changed while the temperature difference and all other parameters were kept fixed. The measured temperature profiles $\Theta(z)$ in the boundary layer obey a power law with an exponent $\alpha \approx 1/2$ that is virtually independent of Γ and Ra. The r.m.s. temperature fluctuation σ is found to decay with increasing distance z from the boundary, according to $\sigma(z) \sim z^\beta$; the value of β is in the range $-0.42 < \beta < -0.30$ and depends both on Ra and Γ. The skewness and kurtosis behave self-similarly in this parameter range. According to the Priestley theory, the global heat flux through the RB cell does not depend on the aspect ratio. It was confirmed by examination of the temperature profiles in the centre of the

cooling plate that both the structure and the thickness of the thermal boundary layer remain nearly unchanged.

In the second series of experiments, covering a range of Ra between 10^{11} and 10^{12} the aspect ratio was maintained constant and the temperature difference was varied from $\Delta\vartheta = 4\,\mathrm{K}$ to $\Delta\vartheta = 62\,\mathrm{K}$. For the lowest temperature difference the mean temperature grows nearly linear with the distance from the cooling plate while for the other cases the profile can be described best by a simple power law. Furthermore it can be stated that a transition of the boundary layer from the laminar to the turbulent type up to $Ra = 10^{12}$ could not be verified despite the fact that the effective exponent in the Nu–Ra relation increases. This result is in a good agreement with theoretical predictions of Kraichnan (1962) and Grossmann & Lohse (2000) and the numerical simulations of Amati *et al.* (2005). Moreover we associate the effect of the enhanced heat transfer in the investigated parameter range with non-Boussinesq effects, with a variation in the fluid properties or potentially with a transition in the global flow structure.

The authors wish to acknowledge the financial support of the Deutsche Forschungsgemeinschaft under grant numbers TH 497/16-1 and 497/16-2 and that of the Thüringer Ministerium für Wissenschaft, Forschung und Kunst for the work reported in this paper. We thank G. Ahlers for useful discussions and V. Mitschunas and H. Hoppe for technical help.

Appendix. Heat transfer

One of the most frequently discussed questions in Rayleigh–Bénard convection concerns the heat transfer through the cell in the highly turbulent regime and its dependence on Ra and Γ. In spite of the fact that our apparatus was not particularly well suited for high-accuracy measurements of the Nusselt number, owing to non-uniformities at the heating plate (see figure 2), we were also interested in this issue and we now address two related questions of particularly interest, as follows.

(i) How does the dimensionless heat transfer Nu depend on the plate distance and on the aspect ratio?

(ii) Can a transition be observed in the exponent of the $Nu(Ra)$ relation at Rayleigh numbers up to 10^{12}, as reported from the Grenoble Group in Chavanne *et al.* (2001)?

In order to answer the first question we compute the Nusselt number from the first series of experiments, where the temperature difference between the heating and the cooling plate was maintained constant at $\Delta T = 40\,\mathrm{K}$ and the aspect ratio was varied between $\Gamma = 1.13$ and $\Gamma = 11.3$. Here the Nusselt number is written as the ratio of the measured total convective heat flow $\dot{Q}_K$ and the diffusive heat flow $\dot{Q}_D$ between both plates:

$$Nu = \frac{\dot{Q}_K}{\dot{Q}_D} = \frac{H\dot{Q}_K}{2\lambda A(\bar{\vartheta}_B - \bar{\vartheta}_{CP})}, \tag{A 1}$$

where λ is the heat conductivity of the air and A denotes the surface area of the cooling plate. Analogously to Ra, Nu is calculated from twice the difference between the bulk temperature $\bar{\vartheta}_B$ and the mean temperature of the cooling plate $\bar{\vartheta}_{CP}$. The convective heat flow $\dot{Q}_K$ is calculated from the measured electrical heating power P, taking into account the heat flow into the ground $\dot{Q}_G$ and the radiation exchange between the heating and the cooling plate $\dot{Q}_R$:

$$\dot{Q}_K = P_{EL} - \dot{Q}_G - \dot{Q}_R. \tag{A 2}$$

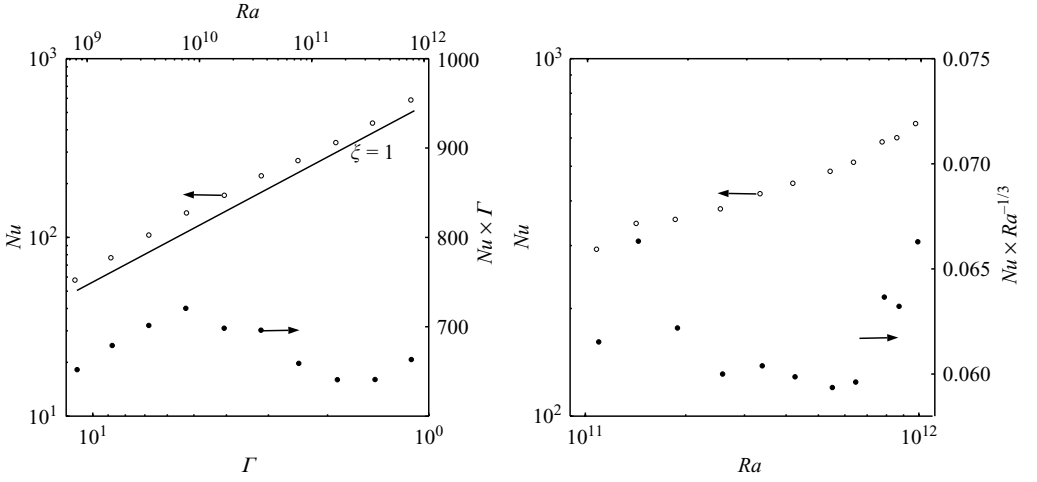

FIGURE 11. The heat transport for variable (left) and constant (right) aspect ratio: the global Nusselt number Nu as obtained from the total heat flux measurements, (A 1), represented in uncompensated (empty circles) and compensated (solid circles) forms.

The electrical heating power was measured by a power meter PM390 with a maximum error of 0.3 %. The heat flow into the ground was computed from a single local-heat-flux measurement in the thermal insulation layer below the heating plate. Owing to the large diameter of the heating plate in comparison with the thickness of the bottom insulation layer, the heat flux into the ground deviates from its mean value only at the edge. Numerical simulations confirmed the correctness of this assumption. The radiation exchange $\dot{Q}_R$ between the plates is determined from a model of two parallel concentric discs with the same diameter D and the distance H as

$$\dot{Q}_R = \frac{\sigma_\epsilon \varepsilon^2 A}{1-(1-\varepsilon)^2 \Phi_{12}} \left(T_{HP}^4 - T_{CP}^4\right) \tag{A 3}$$

with the view factor

$$\Phi_{12} = \frac{1+2R^2-\sqrt{1+4R^2}}{2R^2}, \qquad R = \frac{\Gamma}{2}. \tag{A 4}$$

Here σ_ϵ denotes the Stefan–Boltzmann constant and ε is the emissivity of the surface. The last quantity is measured for $\varepsilon < 0.1$ at several positions of the plates, and so we used this upper limit for all calculations. Since the radiative heat flux between the plates does not exceed 125 W, uncertainties in its calculation are a minor source of error.

In the left-hand diagram in figure 11 the Nusselt number Nu and its value normalized by the reciprocal of Γ are shown for the variable-aspect-ratio series. With only small deviations the dimensionless heat flow can be fitted by the function

$$Nu = C\Gamma^\eta, \qquad C = 655,\ \eta = -0.9770, \tag{A 5}$$

which gives η as very close to -1. Recomputed into a $Nu(Ra)$ power law, (A5) yields $Nu \sim Ra^\xi$ with $\xi = 0.3257$ and confirms that in the highly turbulent regime also the heat flow through the RB cell depends only very weakly on the distance between the plates in the case of a constant temperature difference. Furthermore we compared our results with the widely accepted theory of Grossmann & Lohse (2000)

and found surprisingly good agreement with the predicted value of $\xi_{theor} = 0.323$ in the investigated range of Ra.

For the second series of experiments, where Γ was kept fixed and ΔT was varied, Nu and $Nu/Ra^{1/3}$ are plotted versus Ra in the right-hand part of figure 11. As observed in the low-temperature helium experiments of the Grenoble group, a significant change in the slope of the $Nu(Ra)$ relation exists for $Ra > 7 \times 10^{11}$. This becomes clearer in the compensated plot, where Nu is plotted versus $Ra^{1/3}$. However, because of the unambiguous statement of the unchanged structure of the boundary layer (see § 4) a correlation between this observation and the transition of the turbulent flow towards the ultimate regime can be ruled out. In the interpretation of the increasing exponent in the $Nu(Ra)$ relation we follow Niemela & Sreenivasan (2005), who associated it with non-Boussinesq effects caused by the large temperature difference $\Delta T > 32.2\,\mathrm{K}$ for the corresponding range of Ra. At present we cannot answer this question definitely, but it will be addressed in our future work.

REFERENCES

Amati, G., Koal, K., Massaioli, F., Sreenivasan, K. R. & Verzicco, R. 2005 Turbulent thermal convection at high Rayleigh numbers for a Boussinesq fluid of constant Prandtl number. *Phys. Fluids* **17**, 121701.

Belmonte, A., Tilgner, A. & Libchaber, A. 1993 Boundary layer length scales in thermal turbulence. *Phys. Rev. Lett.* **70**, 4067–4070.

Belmonte, A., Tilgner, A. & Libchaber, A. 1994 Temperature and velocity boundary layers in turbulent convection. *Phys. Rev. E* **50**, 269–279.

Best, A. C. 1935 *Geophys. Mem. Lond* **65**.

Castaing, B., Gunaratne, G., Heslot, F., Kadanoff, L., Libchaber, A., Thomae, S., Wu, X.-Z., Zaleski, S. & Zanetti, G. 1989 Scaling of hard thermal turbulence in Rayleigh–Bénard convection. *J. Fluid Mech.* **204**, 1–30.

Chandrasekhar, S. 1961 *Hydrodynamic and Hydromagnetic Stability*. Clarendon.

Chavanne, X., Chilla, F., Castaing, B., Hébral, B., Chabaud, B. & Chaussy, J. 1997 Observation of the ultimate regime in Rayleigh–Bénard convection. *Phys. Rev. Lett.* **79**, 3648–3651.

Chavanne, X., Chilla, F., Chabaud, B., Castaing, B. & J.Hébral, B. 2001 Turbulent Rayleigh–Bénard convection in gaseous and liquid He. *Phys. Fluids* **13**, 1300–1320.

Chilla, F., Ciliberto, S., Innocenti, C. & Pampaloni, E. 1993 Boundary layer and scaling properties in turbulent thermal convection. *Nuovo Cimento* **15**, 1229.

Chu, T. Y. & Goldstein, R. J. 1973 Turbulent convection in a horizontal layer of water. *J. Fluid Mech.* **60**, 141–159.

Deardorff, J. W. & Willis, G. E. 1967 Investigation of turbulent thermal convection between horizonzal plates. *J. Fluid Mech.* **28**, 675–704.

Grossmann, S. & Lohse, D. 2000 Scaling in thermal convection: a unifying theory. *J. Fluid Mech.* **407**, 27–56.

Fernandes, R. L. J. & Adrian, R. J. 2002 Scaling of velocity and temperature fluctuations in turbulent thermal convection. *Expl Thermal Fluid Sci.* **26**, 355–360.

Fitzjarrald, D. E. 1977 An experimental study of turbulent convection in air. *J. Fluid Mech.* **73**, 693–719.

Fleischer, A. S. & Goldstein, R. J. 2002 High-Rayleigh-number convection of pressurized gases in a horizontal enclosure. *J. Fluid Mech.* **469**, 1–12.

Funfschilling, D. & Ahlers, G. 2004 Plume motion and large-scale circulation in a cylindrical Rayleigh–Bénard cell. *Phys. Rev. Lett.* **92**, 194502.

Haramina, T. & Tilgner, A. 2004 Coherent structures in boundary layers of Rayleigh–Bénard convection. *Phys. Rev.* E **69**, 056306.

Kraichnan, R. H. 1962 Turbulent thermal convection at arbitrary Prandtl number. *Phys. Fluids* **5**, 1374–1389.

Landau, L. D. & Lifschitz, E. M. 1991 *Lehrbuch der Theoretischen Physik, Band IV, Hydrodynamik*. Akademie, Verlag GmbH, Berlin 1991.

Lui, S.-L. & Xia, K.-Q. 1998 Spatial structure of the thermal boundary layer in turbulent convection. *Phys. Rev.* E **57**, 5494–5503.

Malkus, W. V. R. 1954*a* Discrete transistions in turbulent convection. *Proc. R. Soc.* A **225**, 185.

Malkus, W. V. R. 1954*b* The heat transfer and spectrum of thermal turbulence. *Proc. R. Soc.* A **225**, 196.

Niemela, J. J., Skrbek, L., Sreenivasan, K. R. & Donelly, R. J. 2000 Turbulent convection at very high Rayleigh numbers. *Nature* **404**, 837–840.

Niemela, J. J. & Sreenivasan, K. R. 2003 Confined turbulent convection. *J. Fluid Mech.* **481**, 355–384.

Niemela, J. J. & Sreenivasan, K. R. 2005 Turbulent convection at high Rayleigh numbers and aspect ratio 4. *J. Fluid Mech.* **557**, 411–422.

Prandtl, L. 1932 Meteorologische Anwendungen der Stroemungslehre. *Beitr. z. Phys. Atmos.* **19**, 188–202.

Priestley, C. H. B. 1954 Convection from a large horizontal surface. *Austral. J. Phys.* **7**, 176–201.

Priestley, C. H. B. 1959 *Turbulent Transport in the Lower Atmosphere*. University of Chicago Press.

Ramdas, L. A. 1953 *Proc. Ind. Acad. Sci.* **37**, 304–16.

Rider, L. A. & Robinson, G. D. 1951 *Q. J. R. Met. Soc.* **77**, 375–401.

Siggia, E. D. 1994 High Rayleigh number convection. *Annu. Rev. Fluid Mech.* **26**, 137–168.

Shang, X.-D., Qiu, X.-L., Tong, P. & Xia, K.-Q. 2004 Measurement of the local convective heat flux in turbulent Rayleigh–Bénard convection. *Phys. Rev.* E **70**, 026308.

Thomas, D. B. & Townsend, A. A. 1957 Turbulent convection over a heated surface. *J. Fluid Mech.* **2**, 473–492.

Tilgner, A., Belmonte, A. & Libchaber, A. 1993 Temperature and velocity profiles of turbulent convection in water. *Phys. Rev.* E **47**, 2253–2256.

Townsend, A. A. 1958 Temperature fluctuations over a heated horizontal surface. *J. Fluid Mech.* **5**, 209–241.

Verzicco, R. & Camussi, R. 2003 Numerical experiments on strongly turbulent thermal convection in a slender cylindrical cell. *J. Fluid Mech.* **477**, 19–49.

Xia, K.-Q., Sun, C. & Zhou, S.-Q. 2003 Particle image velocimetry measurement of the velocity field in turbulent thermal convection. *Phys. Rev.* E **68**, 066303.